https://doi.org/10.5194/egusphere-2026-1928
Preprint. Discussion started: 29 April 2026

How humidity makes HONO the dominant sink of alkyl substituted Criegee intermediates and a key nocturnal source of OH radicals.

Vishva Jeet Anand[1] and Pradeep Kumar[1]

[1]Department of Chemistry, Malaviya National Institute of Technology Jaipur, Jaipur, 302017,India

Correspondence: Pradeep Kumar (pradeep.chy@mnit.ac.in)

Abstract. Criegee intermediates (CIs) play a key role in the production of OH radicals in the nocturnal environment. It is known that only the unimolecular decomposition of CIs leads to the formation of OH radicals, whereas bimolecular reactions are key for the formation of secondary organic aerosols. In the present work, we have investigated the reactions of CIs (CH_2OO, $(CH_3)_2COO$, anti-CH_3CHOO, and syn-CH_3CHOO) with HONO in the presence of water using quantum chemical calculations and kinetic modelling. The investigation reveals that H_2O catalyzed CI + HONO reactions become a major atmospheric sink for methyl substituted CIs and a prominent source of OH radicals. In the presence of water, CIs loss via CI + HONO reaction is found to be several orders of magnitude higher compared to other traditional sinks such as water and SO_2. For $(CH_3)_2COO$, the H_2O catalysed CI + HONO reaction was found to be $\sim$ 7 orders of magnitude faster than the $H_2O/(H_2O)_2/SO_2$ reactions. Similarly, for syn-CH_3CHOO, the H_2O catalyzed CI + HONO reaction was found to be $\sim$ 8 orders of magnitude faster than the corresponding $H_2O/(H_2O)_2/SO_2$ reactions. The present study reveals that, in the presence of humidity, CI + HONO can control the fate of CIs and act as an efficient route for converting HONO into OH radicals in the absence of light. Incorporation of the kinetics into a global chemical transport model indicates that the water-catalyzed CI + HONO reaction constitutes a major sink (HONO) for Criegee intermediates (CIs), accounting for $\sim$ 60 – 95% of CI loss depending on atmospheric conditions. Globally, this reaction contributes $\sim$ 60% of CH_3CHOO removal, while in the Antarctic winter it dominates CI loss, $\sim$ 95% consumption. In addition, this reaction acts as a source of OH radicals, leading to enhancements of $\sim$ 10% under nocturnal conditions and a global mean increase by $\sim$ 1.6% in OH concentrations.

1 Introduction

Due to the presence of various oxidants, the troposphere acts as a primary shield for living organisms against the pollutants in the atmosphere(Weinstock, 1969; Lelieveld et al., 2004). Among various oxidizing agents, OH radical is the most potent in degrading pollutants in the atmosphere(Lelieveld et al., 2016; Gligorovski et al., 2015). Since a long time it was believed that OH radicals are formed mainly in presence of sunlight via photo-dissociation of species like O_3, H_2O_2, and HONO(Alicke et al., 2003; Aumont et al., 2003; Griffith et al., 2016). Now various studies confirm that OH radicals can also be formed in nocturnal environment(Geyer et al., 2003; Ren et al., 2003; Emmerson and Carslaw, 2009). One of the most important non-photolytic source of OH radicals are Criegee intermediates (CIs)(Novelli et al., 2014; Heard and Pilling, 2003; Kroll et al., 2001). CIs are formed as an intermediate from the ozonolysis of alkenes. This ozonolysis is a highly exothermic reaction that produces energized Criegee intermediates(Alam et al., 2011; Donahue et al., 2011). Although most of these vibrationally hot CIs readily undergo unimolecular dissociation to produce OH radicals, a fraction of them become stabilized through

https://doi.org/10.5194/egusphere-2026-1928
Preprint. Discussion started: 29 April 2026

collisions(Donahue et al., 2011; Novelli et al., 2014; Lester and Klippenstein, 2018). This fraction is highly dependent on the structure of the Criegee intermediates as well as atmospheric conditions. For example, the stabilization fractions are ∼ 35–54% for CH_2OO, ∼ 34% for CH_3CHOO, and ∼24% for $(CH_3)_2COO$(Newland et al., 2020; Nguyen et al., 2015). In fact, under certain atmospheric conditions, fraction of stabilized CIs can be comparable to the vibrationally hot CIs(Newland et al., 2020; Nguyen et al., 2015). The stabilized CIs can undergo either unimolecular dissociation to produce OH radicals or the bimolecular reactions with atmospheric trace gases such as water vapor, SO_2, and NO_2. The bimolecular reactions of CIs play an important role in forming the secondary organic aerosols (SOAs) in the atmosphere(Lin et al., 2016; Onel et al., 2021; Mauldin Iii et al., 2012; Vereecken et al., 2012; Luo et al., 2019). Therefore, a general wisdom for CIs is that unimolecular dissociation contributes to OH radical production, whereas bimolecular reactions of stabilized Criegee intermediate (sCI) lead to the formation of aerosols and acid rains in the atmosphere. Recently, we have proposed that sCI can also produce OH radical via bimolecular reaction with HONO(Anand et al., 2025). Not only that, the study suggests that HONO can be an important sink of CI in areas where HONO is found in high amounts. It is important to note that bimolecular reaction of CI and HONO is a hydrogen atom transfer (HAT) reaction, and is expected to be influenced by various bi-functional catalysts present in the atmosphere. Water vapor is one of the most abundant green house gas in the lower troposphere, with concentrations $\sim 10^{17}$ molecule cm^{-3}(Anglada et al., 2013; Rai and Kumar, 2025b). Water has the ability to accept as well as donate the hydrogen atom and is hence classified as a bi-functional catalyst(Buszek et al., 2011; Kumar and Kumar, 2022). In addition, water can easily form hydrogen bonds with various chemical species and can affect their abundances(Aloisio and Francisco, 1998; Kumar and Sathyamurthy, 2013). Due to the high abundance, bi-functional nature, and ability to form hydrogen bonds, water influences the rates and mechanisms of various gas phase reactions in the atmosphere(Varandas, 2014; Kumar et al., 2016, 2020). Particularly, water plays a significant role in hydrogen atom transfer (HAT) reactions in the atmosphere(Buszek et al., 2012; Rai and Kumar, 2025b). For example, it has been found that for HO_2 + O_3 reaction, the reaction barrier is reduced from 7.16 kcal mol^{-1} to - 2.98 kcal mol^{-1} in the presence of a water molecule(Viegas and Varandas, 2012). Since the title reaction is a hydrogen atom transfer (HAT) reaction, we believe the study of CI + HONO and its real impact in the atmosphere is incomplete without investigating the role of water on the mechanism and kinetics of the title reaction. Therefore, in the present work, we have used the quantum chemical and kinetics calculation to understand the influence of water on mechanism and rate of CI + HONO reaction. The reactivity of CIs is known to be strongly influenced by the substituent attached to the carbon center. To account for these effects, we investigated four representative CIs: the simplest Criegee intermediate (CH_2OO), and dimethyl substituted Criegee intermediate ($(CH_3)_2COO$), and two conformers of single methyl substituted Criegee intermediates, namely anti-CH_3CHOO and syn-CH_3CHOO. Our selection of representative Criegee intermediates for the present study is also motivated by their atmospheric relevance. It is well established that the Criegee intermediates containing up to three carbon atoms are produced mainly from anthropogenic sources in nature(Vereecken et al., 2017), and HONO concentration is higher in the urban areas. Consequently, HONO is supposed to play a major role in deciding the fate of these Criegee intermediates compared to biogenic CIs.

https://doi.org/10.5194/egusphere-2026-1928
Preprint. Discussion started: 29 April 2026

2 Methodology

2.1 Electronic structure calculation

In the present work all the geometries have been optimized using the M06-2X functional in conjunction with the aug-cc-pVTZ basis set. This includes isolated reactants, reactive complexes (RCs), transition states (TSs), product complexes (PCs), and isolated products. To improve the energetics, we carried out single-point energy calculations for the optimized geometries at CCSD(T) level of theory in complete basis set limit (CBS). To estimate the energies at the CCSD(T)/CBS level of theory, first, we calculated the single point energies at CCSD(T)/aug-cc-pVDZ, and CCSD(T)/aug-cc-pVTZ level of theory. These energies were then extrapolated to the corresponding CBS limit using the method of Varandas and Pansini(Varandas and Pansini, 2014; Pansini et al., 2016)(see section S1 of the ESI).

The level of theory CCSD(T)/CBS//M06-2X/aug-cc-pVTZ, was chosen based on previous studies where this level of theory was found to be reasonable for similar reactions(Kumar et al., 2022; Vereecken, 2017; Vereecken et al., 2014; Anand et al., 2025). All electronic structure calculations were carried out using the Gaussian 16 software package(Frisch et al., 2016). Cartesian coordinates and frequencies of all of the optimized geometries provided in the Table S1 in ESI.

2.2 Kinetics calculation

A general reaction scheme for the water monomer (WM) catalyzed reaction paths can be expressed as follows.

$$\mathrm{X + HONO + WM} \underset{k_{-1}}{\overset{k_1}{\rightleftharpoons}} \mathrm{(X\text{-}HONO) + WM} \underset{k_r}{\overset{k_f}{\rightleftharpoons}} \mathrm{RC} \xrightarrow{k_{uni}} \mathrm{TS} \rightarrow \mathrm{PC} \longrightarrow \mathrm{Products} \quad \text{(Path-A)}$$

$$\mathrm{X + HONO + WM} \underset{k_{-1}}{\overset{k_1}{\rightleftharpoons}} \mathrm{(HONO\text{-}WM) + X} \underset{k_r}{\overset{k_f}{\rightleftharpoons}} \mathrm{RC} \xrightarrow{k_{uni}} \mathrm{TS} \rightarrow \mathrm{PC} \longrightarrow \mathrm{Products} \quad \text{(Path-B)}$$

$$\mathrm{X + HONO + WM} \underset{k_{-1}}{\overset{k_1}{\rightleftharpoons}} \mathrm{(X\text{-}WM) + HONO} \underset{k_r}{\overset{k_f}{\rightleftharpoons}} \mathrm{RC} \xrightarrow{k_{uni}} \mathrm{TS} \rightarrow \mathrm{PC} \longrightarrow \mathrm{Products} \quad \text{(Path-C)}$$

Where X denotes CH_2OO/$(CH_3)_2COO$/anti-CH_3CHOO/syn-CH_3CHOO and WM represents H_2O monomer.

As shown above, the reaction is four steps reaction. In the first step, a bimolecular complex is formed between any two of the reactants. In the second step, this bimolecular complex reacts with remained third species to form a termolecular reactive complex (RC). Consequently, depending upon the bimolecular complex form in the first step, the reaction can proceed via three paths, i.e., Path-A, Path-B, and Path-C. In the third step, RC undergoes unimolecular dissociation via transition state (TS) to form the product complex (PC). Finally, PC spontaneously dissociates to form isolated products.

For this kind of reaction, if one assume an equilibrium for the first step, the over all termolecular rate constant (k_t) can be computed via following equation.

$$k_t = K_{eq} \times k_{bi}$$

Where K_{eq} is the equilibrium constant ($K_{eq}=\frac{k_1}{k_{-1}}$) for the first step, and the bimolecular rate constant, i.e., k_{bi} the formation rate of final product from the second step. The equilibrium constants of all the bimolecular complexes have been estimated using THERMO codes as implemented in MultiWell suite of programs(Barker et al., 2021). THERMO uses following equation

https://doi.org/10.5194/egusphere-2026-1928
Preprint. Discussion started: 29 April 2026

to compute the equilibrium constants:

$$K_{eq} = \frac{Q_{XY}}{Q_X Q_Y} \exp\left[\frac{-(E_{XY} - E_X - E_Y)}{RT}\right] \quad \text{(E1)}$$

Here, X and Y represent reactants, while XY denotes the complex formed by the combination of two reactants. Q symbolizes the total partition function of the subscripted species (multiplication of translational, vibrational, rotational, and electronic partition functions), E indicates the energy of the subscripted species.

The bimolecular rate constant (k_{bi}) can be calculated using following equation:

$$k_{bi} = k_f \times \gamma$$

Here, k_f represents the rate of the formation of RC from the reactants (XY, and WM) (capture rate) which is estimated using KTOOLS code as implemented in MultiWell suite of programs(Barker et al., 2021). γ is the product branching ratio for RC computed from the relative yields of reactants (η_{reac}) and products (η_{prod}) starting from the RC, which can be defined as follows:

$$\gamma = \frac{\eta_{prod}}{\eta_{reac} + \eta_{prod}}$$

To calculate γ, we have used master equation approach as implemented in MultiWell code(Barker et al., 2021), where simulations are started from the RC well. Details of master equation calculation is given in the ESI (section S2 of the ESI).

3 Results and discussion

In this section, first we have discussed the uncatalyzed reaction, followed by the water monomer (WM) catalyzed reactions. At last, we compare the uncatalyzed reaction with the catalyzed reaction.

3.1 Uncatalyzed reaction

The energetics and Kinetics of the uncatalyzed reactions between four representative Criegee intermediates (CH_2OO, $(CH_3)_2COO$, anti-CH_3CHOO, and syn-CH_3CHOO) and HONO have been previously investigated at the CCSD(T)/CBS//M06-2X/aug-cc-pVTZ level of theory(Anand et al., 2025). For completeness and comparison, we are summarizing here the results of previous studies. The study showed that, the uncatalyzed reaction with HONO proceeds via hydrogen atom transfer (HAT) path. The effective reaction barriers were calculated to be -8.00 kcal mol^{-1}, -10.14 kcal mol^{-1}, -12.27 kcal mol^{-1}, -8.28 kcal mol^{-1} for CH_2OO + HONO, $(CH_3)_2COO$ + HONO, anti-CH_3CHOO + HONO and syn-CH_3CHOO + HONO reactions, respectively. In addition, in our previous works, we have also calculated rate constants in the 213–320 K temperature range. The calculated rate constants were in the range 1.17×10^{-11} – 6.30×10^{-12} cm^3 molecule^{-1} sec^{-1} for CH_2OO + HONO, 4.28×10^{-11} – 1.63×10^{-11} cm^3 molecule^{-1} sec^{-1} for $(CH_3)_2COO$ + HONO, 9.41×10^{-11} – 7.14×10^{-11} cm^3 molecule^{-1} sec^{-1} for anti-CH_3CHOO + HONO, and 9.18×10^{-12} – 5.53×10^{-12} cm^3 molecule^{-1} sec^{-1} for syn-CH_3CHOO + HONO.

https://doi.org/10.5194/egusphere-2026-1928
Preprint. Discussion started: 29 April 2026

3.2 Catalyzed reaction

We have investigated the WM catalyzed reactions for all four Criegee intermediates, i.e. CH_2OO + HONO, $(CH_3)_2COO$ + HONO, anti-CH_3CHOO + HONO, and syn-CH_3CHOO + HONO reactions. The computed potential energies for all four reaction are depicted in Figures 1 – 4. It is evident from these figures that the mechanisms of all four CIs reactions are similar. The overall reaction can be divided into four steps. In all four cases, reaction can proceeds via three paths, i.e., Path-A, Path-B, and Path-C. For all four reactions, in Path-A, first CI and HONO combines to form a bimolecular complexes, namely CH_2OO–HONO, $(CH_3)_2COO$–HONO, anti-CH_3CHOO–HONO, and syn-CH_3CHOO–HONO with the stabilization energy (with respect to isolated reactants) -10.14 kcal mol^{-1}, -14.20 kcal mol^{-1}, -13.56 kcal mol^{-1}, and -12.42 kcal mol^{-1}, respectively. It is important to note that, CI-HONO bimolecular complex is also the reactive complex for the corresponding uncatalyzed reactions. In Path-B, HONO–WM (stabilizing energy -5.79 kcal mol^{-1}) complex is formed in the first step. In Path-C, CI reacts with WM to form bimolecular complexes, i.e. CH_2OO–WM, $(CH_3)_2COO$–WM, anti-CH_3CHOO–WM, and syn-CH_3CHOO–WM with the stabilization energy -6.78 kcal mol^{-1}, -8.73 kcal mol^{-1}, -8.56 kcal mol^{-1}, and -9.26 kcal mol^{-1}, respectively. In all four cases, in the second step, these bimolecular complexes reacts with the remaining third species to form a termolecular reactive complex namely, RC1, RC2, RC_{anti}, and RC_{syn} with the stabilization energy -17.93 kcal mol^{-1}, -22.61 kcal mol^{-1}, -21.82 kcal mol^{-1}, and -21.22 kcal mol^{-1}, respectively. In the next step, these RCs (RC1, RC2, RC_{anti}, and RC_{syn}) undergo unimolecular transformation via corresponding transition states (TS1, TS2, TS_{anti}, and TS_{syn}) to form respective product complexes (PCs) i.e. PC1, PC2, PC_{anti}, and PC_{syn} with stabilization energy -52.42 kcal mol^{-1}, -44.04 kcal mol^{-1}, -51.05 kcal mol^{-1}, and -47.15 kcal mol^{-1}, respectively. The stabilization observed in all four PCs arises from the formation of a covalent O–H bond between terminal O-atom of CIs and H-atom of HONO. The effective energy barrier of TSs relative to the isolated reactants were computed to be -16.30 kcal mol^{-1}, -18.47 kcal mol^{-1}, -19.51 kcal mol^{-1}, and -17.22 kcal mol^{-1} for TS1, TS2, TS_{anti}, and TS_{syn}, respectively. In the last step, PCs dissociates to form the corresponding final products i.e., CH_2O, $(CH_3)_2CO$, CH_3CHO, $OH^{\bullet}$ and $NO_2^{\bullet}$.

It is evident from the potential energy surfaces (Figures 1 – 4) that the inclusion of WM in the all four reactions results in the lowering of the reaction barrier of the catalyzed paths compare to the corresponding uncatalyzed reactions. Quantitatively, the transition states (TS1, TS2, TS_{anti}, and TS_{syn}) for WM catalyzed path lie at -16.30 kcal mol^{-1}, -18.47 kcal mol^{-1}, -19.51 kcal mol^{-1}, and -17.22 kcal mol^{-1}, respectively, whereas the uncatalyzed path transition states were at -8.00 kcal mol^{-1}, -10.14 kcal mol^{-1}, -12.27 kcal mol^{-1}, and -8.28 kcal mol^{-1}. It suggests that the maximum reduction in barrier height occurs for syn-CH_3CHOO ($\sim$ 9.0 kcal mol^{-1}) followed by $(CH_3)_2COO$ ($\sim$ 8.3 kcal mol^{-1}), CH_2OO ($\sim$ 8.3 kcal mol^{-1}), and anti-CH_3CHOO ($\sim$ 7.3 kcal mol^{-1}). The reactive complexes (RC1, RC2, RC_{anti}, and RC_{syn}) in WM catalyzed path are stabilized by $\sim$ 7.8 kcal mol^{-1}, $\sim$ 8.4 kcal mol^{-1}, $\sim$ 8.3 kcal mol^{-1}, $\sim$ 8.8 kcal mol^{-1}, respectively, compare to the corresponding uncatalyzed path.

It is worth mentioning that the PES contains information only about the enthalpy. In addition to enthalpy, entropy also plays a significant role in chemical reactions. Therefore to assess a realistic impact of WM on the title reaction, we calculated rate constants of the catalyzed reactions. We have calculated the termolecular rate constant (k_t) for the WM catalyzed reaction for

https://doi.org/10.5194/egusphere-2026-1928
Preprint. Discussion started: 29 April 2026

all four representative Criegee intermediates (see Tables S2–S5 of the ESI) in 213–320 K temperature range.

We have calculated the total termolecular rate constant (k_t^{total}=k_t^{Path-A} +k_t^{Path-B} + k_t^{Path-C}) for four representative Criegee intermediates in temperature rang 213–320K. In general, the value of k_t^{total} were found to be highest for $(CH_3)_2COO$ + HONO, followed by syn-CH_3CHOO + HONO, anti-CH_3CHOO + HONO, and CH_2OO + HONO. For example, at 298 K, the computed values of k_t^{total} are 1.10×10^{-27} cm^6 $molecule^{-2}$ s^{-1}, 9.83×10^{-28} cm^6 $molecule^{-2}$ s^{-1}, 4.31×10^{-28} cm^6 $molecule^{-2}$ s^{-1}, and 1.52×10^{-30} cm^6 $molecule^{-2}$ s^{-1}, for WM catalyzed $(CH_3)_2COO$ + HONO, syn-CH_3CHOO + HONO, anti-CH_3CHOO + HONO, and CH_2OO + HONO reactions, respectively. As far as the individual contribution of various paths are concern, one can see from Table S2 that for all four CIs reactions, Path-A is the major contributor to the k_t^{total}. For example at 298 K, the termolecular rate constant for Path-A, Path-B, and Path-C are 1.38×10^{-30} cm^6 $molecule^{-2}$ s^{-1}, 5.96×10^{-32} cm^6 $molecule^{-2}$ s^{-1}, and 7.82×10^{-32} cm^6 $molecule^{-2}$ s^{-1}, respectively for CH_2OO + HONO reaction. A similar trend is observed for $(CH_3)_2COO$, anti-CH_3CHOO, and syn-CH_3CHOO, with Path-A dominating Path-B, and Path-C by 1–3 orders of magnitude.

3.3 Catalyzed vs Uncatalyzed reaction

It is important to note that the uncatalyzed reaction is bimolecular, while the catalyzed reaction is a termolecular reaction. Therefore, for an appropriate comparison between the rate constant of the catalyzed and uncatalyzed reaction, both the bimolecular rate constant and termolecular rate constant are converted into the effective unimolecular rate constant (k_{eff}) by multiplying the concentration of corresponding co-reactants. For the uncatalyzed reaction, bimolecular rate constants are multiplied by the concentration of HONO, whereas for the catalysed paths, termolecular rate constants are multiplied by the concentration of both the co-reactants, i.e., WM and HONO. It is important to note that Criegee intermediates containing more than three carbon atoms dominantly occur in anthropogenic environments(Vereecken et al., 2017). Therefore, an average HONO concentration (8.8×10^{10} molecule cm^{-3})(Pawar et al., 2024) under urban conditions is taken. The concentration of water vapor, exhibits significant variability in the atmosphere, depending on the saturation vapor pressure and relative humidity (RH). Therefore, two representative H_2O concentrations are considered: one corresponding to 20% RH and the other to 100% RH. The 20% RH serves as the lower limit and 100% RH represents the upper limit water vapor concentration in the present work.

The effective rate constants of catalyzed reaction are tabulated in Tables 1 – 4 in temperature range 213–320 K, along with the same for uncatalyzed reactions. The reactivity of CIs are highly dependent on their molecular structure; consequently, the role of WM catalysis in these reactions also depends strongly on structure of CIs. For WM catalyzed CH_2OO + HONO reaction, Table 1 shows that in the whole temperature range uncatalyzed effective rate constant is dominant over the catalysed path. Even at high humidity conditions (RH=100%) uncatalyzed effective rate is 4–8 times higher than that of the WM catalyzed reaction. Under low humidity conditions (RH=20%), this dominance is more pronounced, i.e. k_{eff} for uncatalyzed reaction becomes 20–40 times higher than the WM catalysed reaction. For example, at 298 K, k_{eff} of catalyzed paths at RH=20% and RH=100% are found to be 2.04×10^{-2} s^{-1} and 1.02×10^{-1} s^{-1}, respectively, while same for uncatalyzed is 6.41×10^{-1} s^{-1}. In contrast, for remaining three WM catalysed reaction, i.e. $(CH_3)_2COO$ + HONO, anti-CH_3CHOO + HONO, and syn-

https://doi.org/10.5194/egusphere-2026-1928
Preprint. Discussion started: 29 April 2026

CH_3CHOO + HONO, catalysed reactions dominant over the corresponding uncatalyzed reactions.
For WM catalyzed $(CH_3)_2COO$ + HONO reaction, (Table 2) in whole temperature range catalysed path dominant over the uncatalyzed path at both, lower as well as high humidity conditions. At high humidity (RH=100%) catalysed path is $\sim$ 2–3 orders of magnitude higher than the uncatalyzed reaction. Even at low humidity (RH=20%) catalysed path dominant over the uncatalyzed path by $\sim$ 1–2 orders of magnitude. For example at 298 K, k_{eff} for catalyzed path at RH=20% and RH=100% were found to be 14.8 and 74.2 s^{-1}, while same for the uncatalyzed reaction is only 1.8 s^{-1}. One can also see from Table 2 that the dominance of catalyzed path increases with decreasing temperature. For example, for the uncatalyzed path, the k_{eff} are 3.8 s^{-1} and 1.44 s^{-1} at 213 and 320 K, respectively, which increase to 623 s^{-1} and 6.02 s^{-1} at 213 K and 320 K, respectively even with 20% humidity.
Similarly, for WM catalyzed anti-CH_3CHOO + HONO, and syn-CH_3CHOO + HONO reactions, the k_{eff} of the catalyzed paths at high humidity (RH = 100%) are larger than the uncatalyzed reactions by $\sim$ 1–3 and 2–4 orders of magnitude, respectively (Table 3, and Table 4). Even under low-humidity conditions (RH = 20%), the catalyzed anti-CH_3CHOO + HONO reaction remains about a factor of $\sim$ 20 times faster than the uncatalyzed reaction at lower temperature (at 213 K) and becomes competitive at higher temperatures (above 290 K). For the syn-CH_3CHOO + HONO reaction, even at low humidity, the WM-catalyzed effective rate constants dominate the uncatalyzed reaction by $\sim$ 1–3 orders of magnitude across the entire temperature range. For example, at 298 K the effective rate constants for the WM-catalyzed syn-CH_3CHOO + HONO reaction are 13.2 s^{-1} at RH=20% and 66.0 s^{-1} at RH=100%, whereas the corresponding uncatalyzed effective rate constant is only 0.56 s^{-1}.

4 Atmospheric Implication

To assess the atmospheric relevance of the title reaction, it is necessary to carry out a comparative study with other known sinks of Criegee intermediates. The major known sinks of CIs in the atmosphere are water and SO_2(Lin et al., 2016; Mauldin Iii et al., 2012). Therefore, we have compared k_{eff} of these bimolecular sinks (H_2O, $(H_2O)_2$ and SO_2) of Criegee intermediate with the all four reactions investigated in the present work. In Figure 5a, we have compared the k_{eff} of WM catalyzed CH_2OO + HONO reaction with the k_{eff} of CH_2OO + WM/WD/SO_2 reactions (at 20% RH and 100% RH). As shown in Figure 5a, k_{eff} of CH_2OO + WD is the dominant reaction across the entire temperature range (213–320 K), followed by CH_2OO + WM, and CH_2OO + SO_2 reactions. It suggests that in the presence of water HONO is only a minor sink of CH_2OO.
Similarly, we have compared remaining three WM catalysed reactions ($(CH_3)_2COO$ + HONO, anti-CH_3CHOO + HONO, and syn-CH_3CHOO + HONO) with the other known bimolecular sinks of CIs (Tables S7–S9 of ESI, and Figures 5b – 5d). Figure 5b depicts a comparison of the k_{eff} for the WM-catalyzed $(CH_3)_2COO$ + HONO reaction with other competing sinks (WM, WD, and SO_2) reactions. It is evident from Figure 5b that WM assisted $(CH_3)_2COO$ + HONO reaction is completely dominant in the entire temperature range (213–320 K) in low as well as in high humidity conditions. In fact, one can see from Figure 5b that WM catalysed reaction also dominant the unimolecular decay of $(CH_3)_2COO$ below 290 K. The dominance of the WM catalyzed reaction becomes more pronounced at lower temperatures and higher humidity. Quantitatively, at 100% RH (20%

https://doi.org/10.5194/egusphere-2026-1928
Preprint. Discussion started: 29 April 2026

RH), the competing $(CH_3)_2COO$ + WD reaction is $\sim$ 7 ($\sim$ 6) orders of magnitude slower than WM catalyzed $(CH_3)_2COO$ + HONO reaction. It clearly indicates that, in presence of water $(CH_3)_2COO$ + HONO reaction is the major atmospheric sink of $(CH_3)_2COO$.

Figure 5c and Figure 5d depict the comparison of k_{eff} of WM-catalyzed anti/syn-CH_3CHOO + HONO reaction with the other sinks of CIs. It is evident from the Figure 5c that, at 100% RH, WM-catalyzed anti-CH_3CHOO + HONO reaction becomes dominant compared to the other sinks only below 250 K, whereas at 20% RH it dominant only below 235 K. It is also evident Figure 5c that in higher temperature region, after WD, WM catalysed HONO reaction is the dominant reaction for anti-CH_3CHOO. Figure 5d shows that unlike, anti-CH_3CHOO, in the case of WM-catalyzed syn-CH_3CHOO + HONO reaction, it is the dominant sink in the entire temperature range at low as well as at high humidity conditions. In fact, at the lower temperatures (below 250 K) it becomes 8–10 orders higher compared to the WD and WM reactions. More importantly, it dominates even unimolecular decay below 290 K. Consequently, in the presence of WM, syn-CH_3CHOO + HONO reaction becomes the major atmospheric sink of syn-CH_3CHOO. It is important to note that syn-CH_3CHOO conformer is thermodynamically more stable than the anti-CH_3CHOO conformer. As a result, the syn-CH_3CHOO conformer is form above 80% relative to the total CH_3CHOO(Nakajima et al., 2015; Nakajima and Endo, 2014). Therefore, the syn-CH_3CHOO conformer dominates the atmospheric abundance of CH_3CHOO Criegee intermediate.

To further illustrate the importance of water catalyzed CIs + HONO, we computed the branching fractions (20% RH and 100% RH) for the WM catalyzed reactions of all four CIs (see Figure 6). To calculate the branching fraction, we have used the k_{eff} for the following CI reaction: CI + (H_2O), CI + $(H_2O)_2$, uncatalysed CI + HONO, and WM catalysed CI + HONO reactions. The CI + SO_2 reaction was not included in the branching fraction calculation due to the sparse availability of SO_2 data. Moreover, inclusion of the CI + SO_2 reaction does not much affect the calculated branching fractions. The branching fraction for the WM catalysed CI + HONO reaction was calculated as

$$\text{Branching Fraction} = \frac{k_{\text{eff}}^{\text{CI+HONO+WM}}}{k_{\text{eff}}^{\text{CI+(H}_2\text{O)}} + k_{\text{eff}}^{\text{CI+(H}_2\text{O)}_2} + k_{\text{eff}}^{\text{CI+HONO}} + k_{\text{eff}}^{\text{CI+HONO+WM}}}$$

It is evident from Figure 6a that, for CH_2OO, the WM catalyzed reaction is negligible at higher temperatures and becomes a minor sink only below 240 K, contributing $\sim$ 4% and 8%, at 20% and 100% RH, respectively. In contrast, for $(CH_3)_2COO$, the WM catalyzed reaction contributes significantly in the entire temperature range (213–320 K) at low as well as high humidity. Figure 6b clearly suggests that below 280 K, this reaction becomes completely dominant, with the branching fraction approaching 1, indicating that HONO acts as exclusive sink of $(CH_3)_2COO$. Figures 6c and 6d further show that WM catalyzed reactions are also important for anti/syn-CH_3CHOO. For anti-CH_3CHOO, branching fraction becomes 0.2 below 250K and increases rapidly with decreasing temperature. In fact, below 240 K the contribution of this reaction becomes 80–100%. For syn-CH_3CHOO, the WM catalyzed reaction is significant under both low and high humidity conditions. It becomes a major contributor below 270 K ($\sim$ 70–100 %) at 20% RH, and it becomes the exclusive contributor below 280 K at 100% RH. After establishing that HONO can be a major sink of methyl substituted Criegee intermediates at low temperatures, it is important to discuss the products of this reaction. The products of this reaction are $OH^{\bullet}$, HCHO, $(CH_3)_2CO$, CH_3CHO, and $NO_2^{\bullet}$. In fact

https://doi.org/10.5194/egusphere-2026-1928
Preprint. Discussion started: 29 April 2026

unlike unimolecular decay, where CI is the source of OH radical here CI is a co-reactant and HONO is the actual source of OH radicals. An isotopic labelling experiment can be used to differentiate the two reactions. Therefore CI + HONO reaction provided a route to convert HONO into OH radical in the absence of light. It also suggests that HONO, which is normally more important in daytime chemistry, can be key for nocturnal formation of OH radicals. In fact, other products of this reaction, i.e., HCHO, $(CH_3)_2CO$, CH_3CHO, and $NO_2^\bullet$ are also important as it is known that they readily react with HO_2 radicals via following reactions. HCHO/$(CH_3)_2CO$ + $HO_2^\bullet$ $\longrightarrow$ $HOCH_2OO$/$(CH_3)_2C(OH)OO$ (Gao et al., 2024; Hermans et al., 2004; Rai and Kumar, 2025a) and $NO_2^\bullet$ + $HO_2^\bullet$ $\longrightarrow$ HO_2NO_2(Christensen et al., 2004). Consequently, the CI + HONO reaction provides an interconversion mechanism to $OH^\bullet \leftrightarrow HO_2^\bullet$.

5 Atmospheric modelling

To further assess the impact of WM catalyzed CI + HONO reaction on the global budget of Criegee intermediates and OH radicals, we performed atmospheric model simulations using the GEOS-Chem chemical transport model(Bey et al., 2001). Simulations were conducted with the global 3D atmospheric chemistry transport model (CTM) GEOS-Chem (version 14.7.0). The model integrates meteorological data from the NASA Modern-Era Retrospective Analysis for Research and Applications (MERRA-2) with a 4.0° x 5.0° spatial resolution and 72 vertical levels. Emissions were calculated using the standard Harmonized Emissions Component (HEMCO). Gas-phase chemistry was simulated using the Kinetic Pre-Processor (KPP). To evaluate seasonal variability, simulations were performed for two representative days corresponding to 1 January (winter) and 1 June (summer). The model was first executed using the standard (base) chemical mechanism. Subsequently, the mechanism was updated to include the additional water catalyzed reactions of CH_2OO and CH_3CHOO with HONO (full reaction details are provided in Table S10 in the ESI). The Criegee intermediate ($(CH_3)_2COO$) was not included in the simulations, as it is not part of the default chemical mechanism in the current version of GEOS-Chem.

We first discuss the impact of title reaction on global budget of CIs followed by the impact of same on OH radicals budget. Figures 7a and 7b present the 24-hour simulations for January and June, respectively. These figures show the relative change in the concentration of CH_3CHOO upon inclusion of the HONO reactions in the model. As shown in Figure 7a, the maximum decrease in CH_3CHOO concentration during the January simulation is $\sim$ 59.2%, indicating that HONO acts as a major sink for CH_3CHOO under these conditions. Regionally, the change in concentration of CH_3CHOO ranges from 15% – 60% over Asia and Russia. In the United States the same decrease in range 15% –30% while in the Antarctic region the decrease is about $\sim$ 15%. In contrast, the June simulation (Figure 7b) shows a much larger maximum reduction (up to $\sim$ 95%), suggesting that the title reaction becomes the dominant, and in some regions nearly the exclusive, sink of CH_3CHOO. This enhanced effect is due to the contribution from polar winter conditions in Antarctica during June, where long darkness suppresses photochemical dissociation of HONO, and hence allowing a build up of HONO concentration. We also estimated the changes in CH_2OO concentrations (Figure S5 in ESI). The model simulations show negligible changes in its atmospheric concentration. This result is consistent with our kinetic results indicating that HONO is only a minor sink of CH_2OO.

In addition to CI loss, the reaction of HONO with Criegee intermediates leads to the formation of OH radicals. Therefore, we

https://doi.org/10.5194/egusphere-2026-1928
Preprint. Discussion started: 29 April 2026

also evaluated the impact of these reactions on atmospheric OH concentrations using 24-hour simulations for both January and June. As shown in Figure 8a, the global average OH concentration increases by about $\sim$ 1.58% in the January simulation. Regionally, enhancements in OH are observed in areas where CH_3CHOO consumption is significant (Alaska (USA), Asia, Russia and Arctic Circle). For the June simulation (Figure 8b), the increase in OH concentration reaches up to $\sim$10.8%, again driven primarily by conditions in the Antarctic region, where extended periods of darkness favor HONO-mediated dark reaction chemistry. Overall, these results indicate that water mediated CI + HONO reaction is more crucial as a source of OH radical in nighttime.

To further investigate the impact of the CI + HONO reactions under nocturnal conditions, we performed additional 6-hour simulations focused on nighttime periods in selected regions. For Asian regions (China, India, and east-central Russia), the simulation window was defined as 15:00–21:00 UTC, corresponding to local nighttime ($\sim$ 23:00 – 05:00 in China and Russia, and 20:30 – 02:30 in India). For the United States (Eastern Standard Time, EST), the simulation period was set to 03:00 – 09:00 UTC, corresponding to 23:00 – 05:00 local nighttime. These simulations were conducted for both January and June to cover seasonal variability. As shown in Figure 9a, the January nighttime simulation over Asian regions results in an increase in OH concentrations $\sim$ 10%. The increament is localized to regions experiencing nighttime conditions, while negligible changes are observed elsewhere. For the U.S. (EST) nighttime case (Figure 9b), the maximum increase is smaller ($\sim$ 4.7%), consistent with comparatively lower HONO concentrations in this region. In June, similar simulations were performed using the same regional time windows. Figure 9c shows that the largest increase in OH ($\sim$ 10.2%) occurs over the Antarctic region, which is in winter during this period and characterized by long darkness. In contrast, the increases over Asian nighttime regions are smaller than in January, reflecting shorter dark hours durations and relatively higher temperatures during summer. A similar pattern is observed for the U.S. nighttime case (Figure 9d), where the maximum increase ($\sim$ 10.3%) again occurs over Antarctica.

6 Conclusions

In this work, we investigate the influence of water on the reaction of HONO with four different Criegee intermediates. The present investigation suggests that, for the simplest Criegee intermediate (CH_2OO), WD remains the dominant sink, and CH_2OO + HONO becomes a minor contributor only at low temperature and high humidity. In contrast, for $(CH_3)_2COO$, the WM catalyzed reaction with HONO becomes the dominant atmospheric sink over the entire temperature range (213–320 K) under both low and high humidity conditions. It is dominant the other sinks such as water and SO_2 by $\sim$ 6–7 orders of magnitude. Similarly, for the syn-CH_3CHOO, the presence of humidity makes HONO also the dominant sink in the whole temperature range. For anti-CH_3CHOO, the WM-catalyzed HONO reaction becomes the dominant sink below 250 K at 100% RH, while at 20% RH it dominates only below 235 K. These results suggest that, in the presence of water, CIs + HONO reactions can serve as the most significant atmospheric sinks for certain CIs. It is important to note that in the present study, the average HONO concentration (8.8×10^{10} molecule cm^{-3}) under urban conditions is taken. In forested regions, HONO concentrations are typically about two orders of magnitude lower ($\sim 10^8$ molecule cm^{-3}). Even at this lower concentration, the WM catalyzed $(CH_3)_2COO$ + HONO and syn-CH_3CHOO + HONO reactions will remain dominant than the H_2O and SO_2

https://doi.org/10.5194/egusphere-2026-1928
Preprint. Discussion started: 29 April 2026

sinks. Thus, this study reveals that, in the presence of water, CI + HONO reactions are the dominant atmospheric sinks for certain CIs in both urban and forest environments.

In addition, the present investigation also suggests that the title reaction can be an important source of $OH^{\bullet}$ in the nocturnal atmosphere. Beyond energetics and kinetics results, global atmospheric modeling indicates that inclusion of the water mediated CI + HONO reaction, HONO become a dominant sink for Criegee intermediates (CIs) while simultaneously act as a source of OH radicals. Incorporation of this reaction into the base chemical mechanism significantly alters the atmospheric fate of CIs. Model simulation show that HONO acts as a major sink for CIs, accounting for $\sim 60\%$ of CH_3CHOO removal. In the Antarctic region in winter season long dark hours, this reaction becomes the predominant, and $\sim 95\%$ CIs consume, leading to an almost complete depletion of CIs. Furthermore, the title reaction contributes to OH radical formation. Simulations reveal an enhancement of $\sim 10\%$ in OH production under nocturnal conditions, along with a global mean increase of $\sim 1.6\%$ in OH concentrations. Moreover, the products of CIs + HONO reaction can act as a sink for $HO_2^{\bullet}$ radicals, and hence this reaction is capable of $OH^{\bullet} \leftrightarrow HO_2^{\bullet}$ recycling.

Data availability. All data supporting the findings of this study are available in the Supplementary Information file.

Author contributions. VJA: Conducted the investigation, Writing–original draft, Formal analysis, curated the data. PK: Provided supervision, resources, and methodology; conceptualized the study; acquired funding; and contributed to the review and editing of the manuscript.

Competing interests. The authors declare that they have no conflict of interest.

7 Acknowledgment

V.J.A. acknowledge MNIT Jaipur for financial assistance. P.K. acknowledges DST, Govt. of India, for the financial support through the sanctioned project No. EEQ/2023/000351.

https://doi.org/10.5194/egusphere-2026-1928
Preprint. Discussion started: 29 April 2026

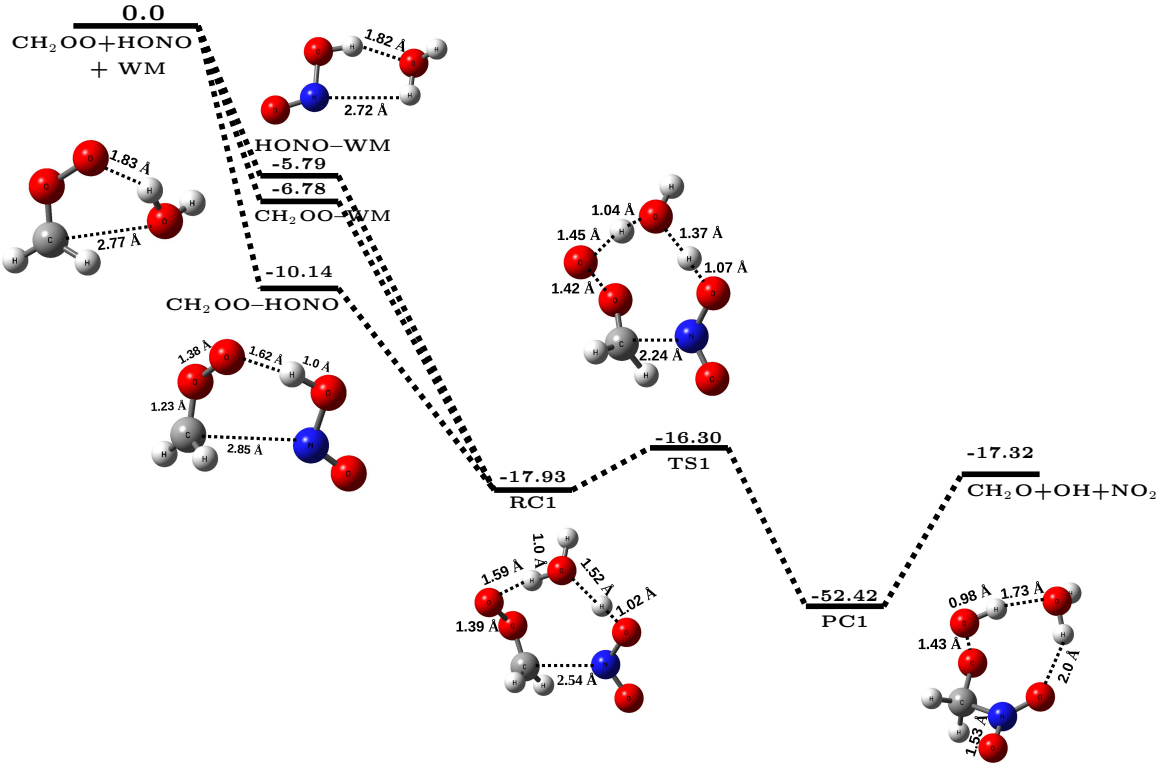

Figure 1. The potential energy surface for CH_2OO + HONO +WM reaction (in kcal mol^{-1}) obtained at CCSD(T)/CBS//M06-2X/aug-cc-pVTZ level of theory along with optimized geometries of species involved in the reaction.

https://doi.org/10.5194/egusphere-2026-1928
Preprint. Discussion started: 29 April 2026

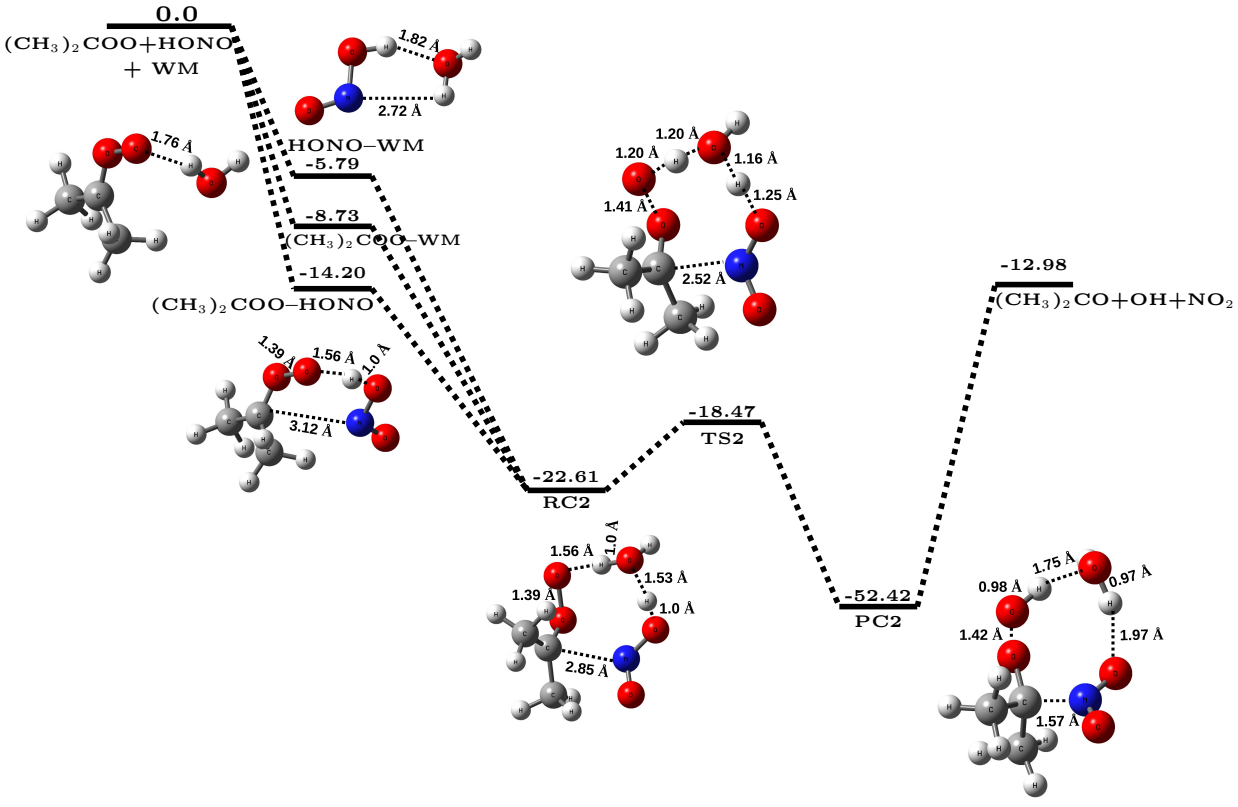

Figure 2. The potential energy surface for $(CH_3)_2OO$ + HONO + WM reaction (in kcal mol^{-1}) obtained at CCSD(T)/CBS//M06-2X/aug-cc-pVTZ level of theory along with optimized geometries of species involved in the reaction.

https://doi.org/10.5194/egusphere-2026-1928
Preprint. Discussion started: 29 April 2026

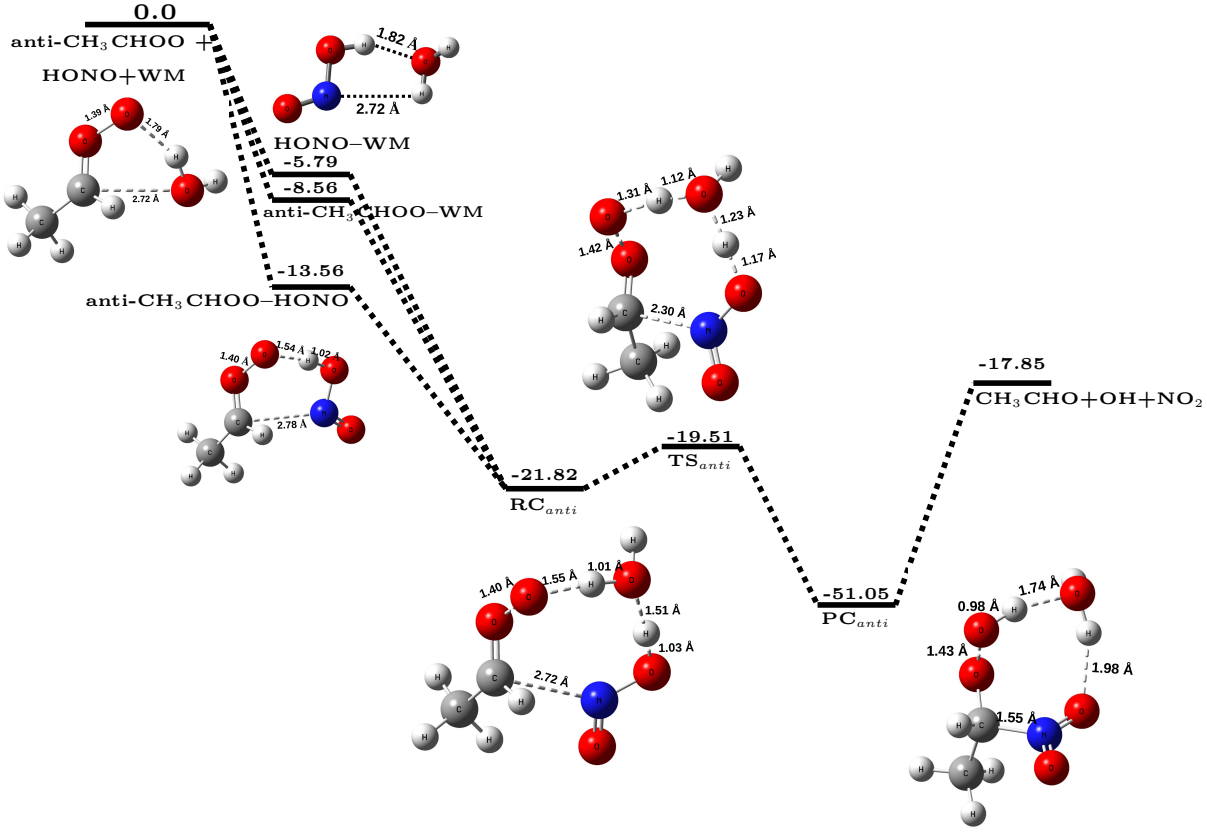

Figure 3. The potential energy surface for anti-CH_3CHOO + HONO + WM reaction (in kcal mol^{-1}) obtained at CCSD(T)/CBS//M06-2X/aug-cc-pVTZ level of theory along with optimized geometries of species involved in the reaction.

https://doi.org/10.5194/egusphere-2026-1928
Preprint. Discussion started: 29 April 2026

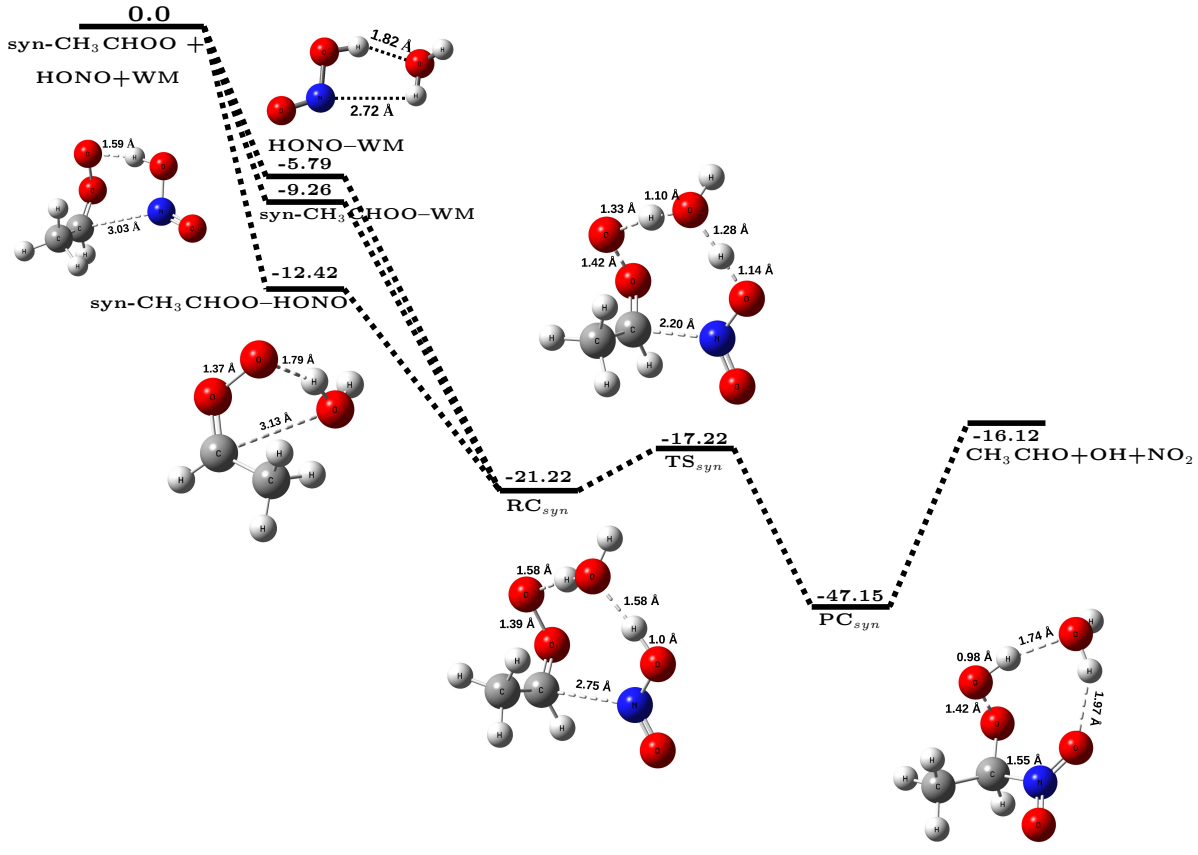

Figure 4. The potential energy surface for syn-CH_3CHOO + HONO + WM reaction (in kcal mol^{-1}) obtained at CCSD(T)/CBS//M06-2X/aug-cc-pVTZ level of theory along with optimized geometries of species involved in the reaction.

https://doi.org/10.5194/egusphere-2026-1928
Preprint. Discussion started: 29 April 2026

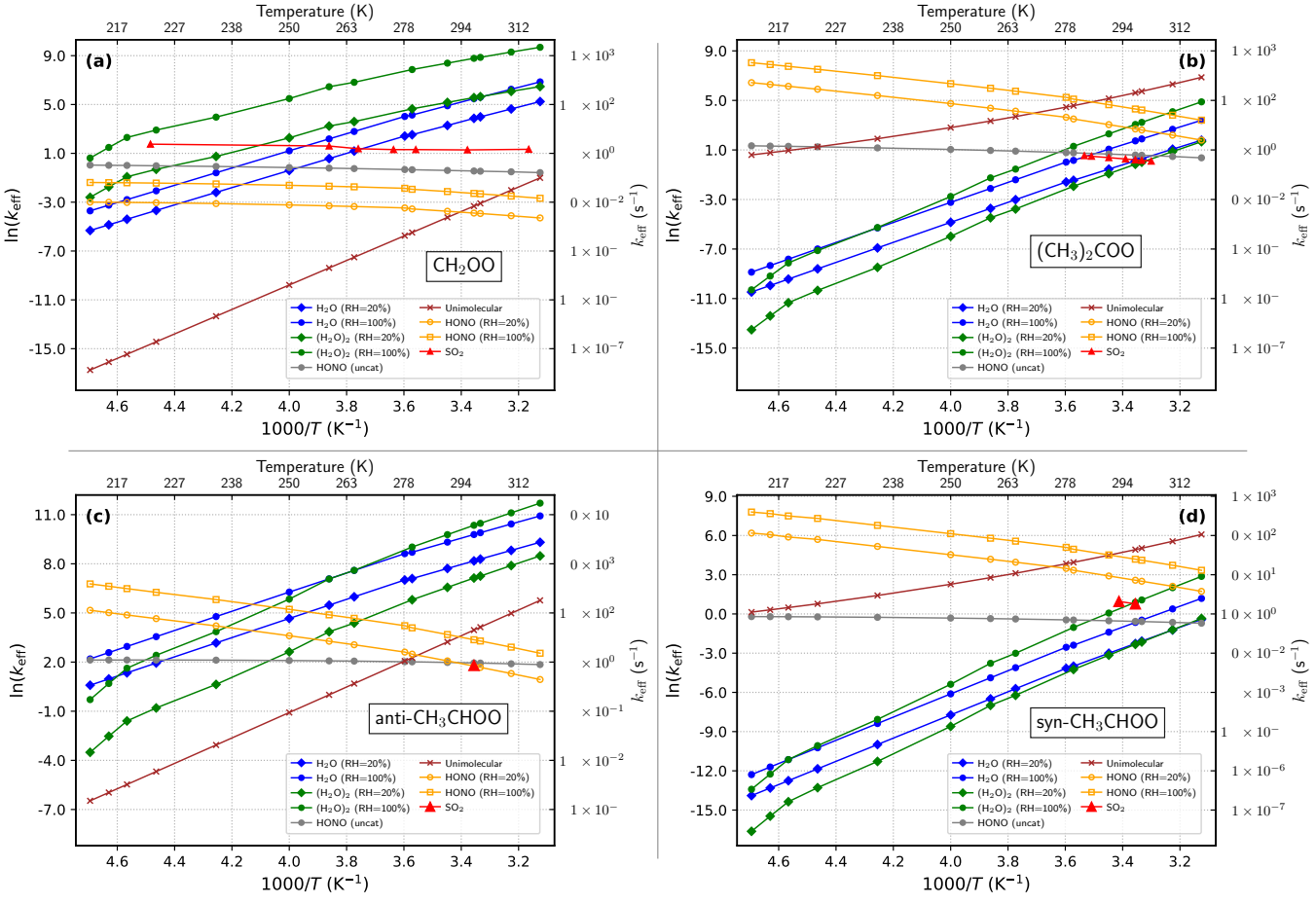

Figure 5. Effective rate constant comparison (k_{eff}, in sec^{-1}) for the WM catalyzed CIs + HONO and other known CIs sinks (H_2O, $(H_2O)_2$, SO_2, unimolecular decay, and uncatalysed CI + HONO) at 20% and 100% relative humidity over the temperature range 213–320 K.

https://doi.org/10.5194/egusphere-2026-1928
Preprint. Discussion started: 29 April 2026

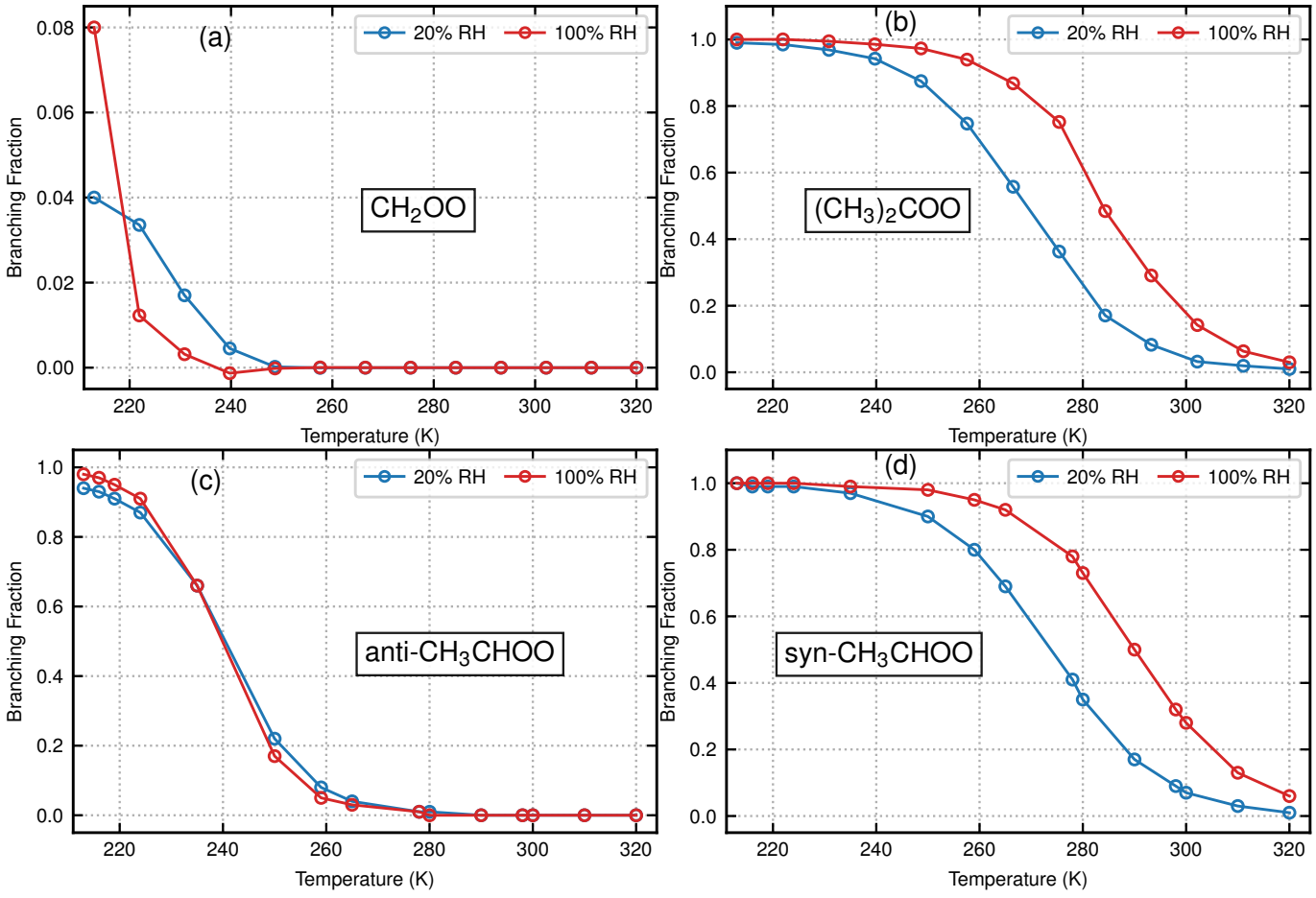

Figure 6. Temperature dependent branching fractions calculated from effective rate constants for the WM catalysed CI + HONO reaction at 20% and 100% relative humidity over the temperature range 213–320 K.

https://doi.org/10.5194/egusphere-2026-1928
Preprint. Discussion started: 29 April 2026

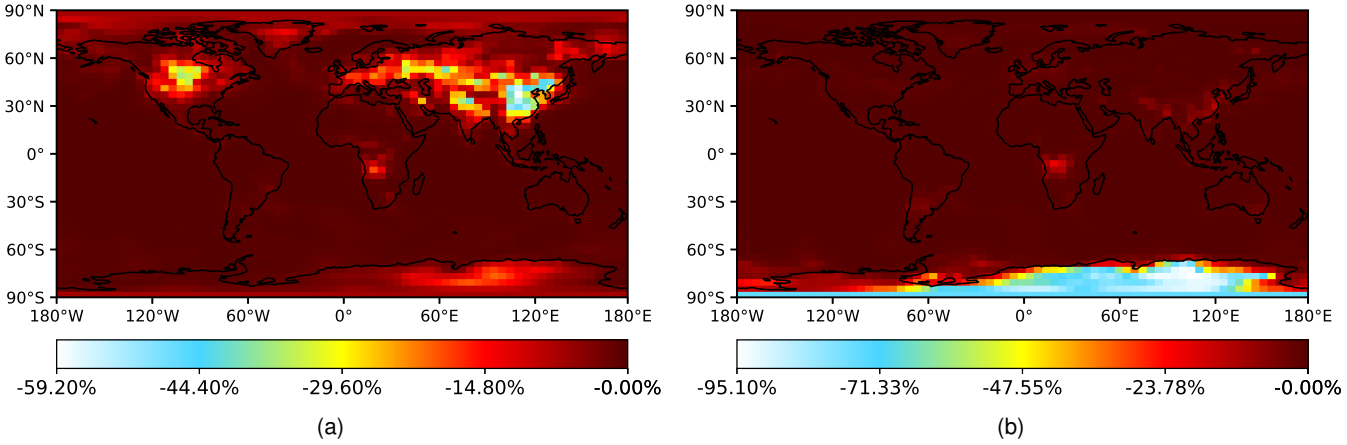

Figure 7. Global relative changes in CH_3CHOO concentrations resulting from the inclusion of the water catalyzed (WM) CI + HONO reaction in 24-hour simulations. (a) CH_3CHOO changes in January, (b) CH_3CHOO changes in June.

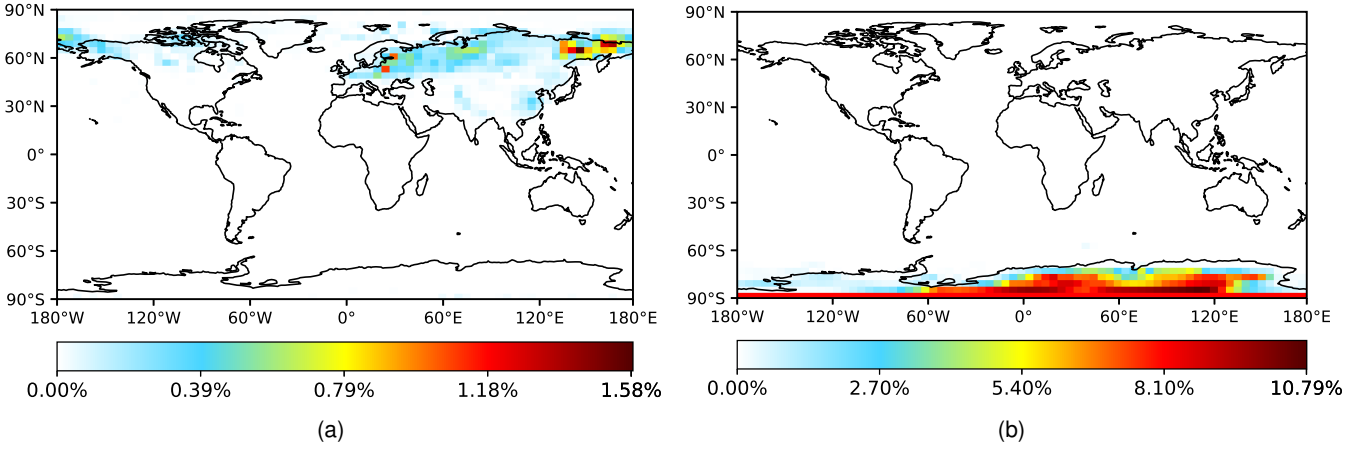

Figure 8. Global relative changes in OH concentrations resulting from the inclusion of the water catalyzed (WM) CI + HONO reaction in 24-hour simulations. (a) OH changes in January, and (b) OH changes in June.

https://doi.org/10.5194/egusphere-2026-1928
Preprint. Discussion started: 29 April 2026

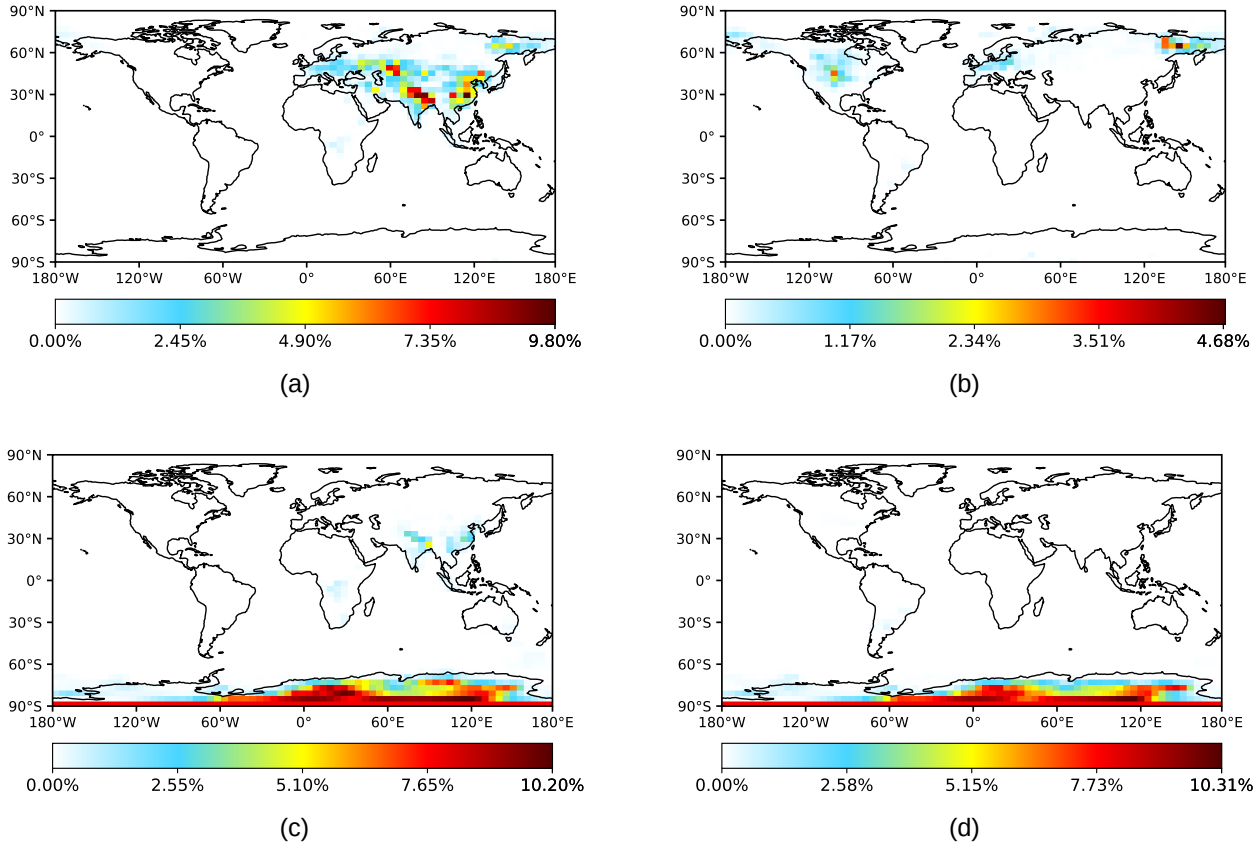

Figure 9. Global changes in OH concentrations due to the inclusion of the water catalyzed (WM) CI + HONO reaction during 6-hour nighttime simulations. (a) January nighttime conditions over India, China, and east-central Russia (b) January nighttime conditions over the United States (c) June nighttime conditions over India, China, and east-central Russia and (d) June nighttime conditions over the United States.

https://doi.org/10.5194/egusphere-2026-1928
Preprint. Discussion started: 29 April 2026

Table 1. Effective rate constants (k_{eff}, in sec^{-1}) for CH_2OO + HONO + WM reaction within the temperature range of 213–320 K, with WM at 20% and 100% relative humidity (RH).

Temp.	$k_{eff}^{RH=20\%}$	$k_{eff}^{RH=100\%}$	k_{eff}^{uncat}
213	5.01×10^{-2}	2.50×10^{-1}	1.04
216	4.95×10^{-2}	2.47×10^{-1}	1.02
219	4.88×10^{-2}	2.44×10^{-1}	1.01
224	4.76×10^{-2}	2.38×10^{-1}	9.81×10^{-1}
235	4.45×10^{-2}	2.22×10^{-1}	9.25×10^{-1}
250	3.97×10^{-2}	1.98×10^{-1}	8.51×10^{-1}
259	3.68×10^{-2}	1.84×10^{-1}	8.08×10^{-1}
265	3.49×10^{-2}	1.75×10^{-1}	7.81×10^{-1}
278	3.11×10^{-2}	1.55×10^{-1}	7.23×10^{-1}
280	2.86×10^{-2}	1.43×10^{-1}	7.14×10^{-1}
290	2.37×10^{-2}	1.19×10^{-1}	6.73×10^{-1}
298	2.04×10^{-2}	1.02×10^{-1}	6.41×10^{-1}
300	1.97×10^{-2}	9.85×10^{-2}	6.33×10^{-1}
310	1.64×10^{-2}	8.21×10^{-2}	5.95×10^{-1}
320	1.37×10^{-2}	6.86×10^{-2}	5.60×10^{-1}

https://doi.org/10.5194/egusphere-2026-1928
Preprint. Discussion started: 29 April 2026

Table 2. Effective rate constants (k_{eff}, in sec^{-1}) for $(CH_3)_2COO$ + HONO + WM reaction within the temperature range of 213–320 K, with WM at 20% and 100% relative humidity (RH).

Temp.	$k_{eff}^{RH=20\%}$	$k_{eff}^{RH=100\%}$	k_{eff}^{uncat}
213	6.23×10^{2}	3.12×10^{3}	3.80
216	5.38×10^{2}	2.69×10^{3}	3.71
219	4.64×10^{2}	2.32×10^{3}	3.64
224	3.66×10^{2}	1.83×10^{3}	3.50
235	2.20×10^{2}	1.10×10^{3}	3.21
250	1.15×10^{2}	5.73×10^{2}	2.83
259	7.92×10^{1}	3.96×10^{2}	2.61
265	6.24×10^{1}	3.12×10^{2}	2.47
278	3.80×10^{1}	1.90×10^{2}	2.19
280	3.31×10^{1}	1.65×10^{2}	2.15
290	2.10×10^{1}	1.05×10^{2}	1.95
298	1.48×10^{1}	7.42×10^{1}	1.80
300	1.36×10^{1}	6.82×10^{1}	1.77
310	8.99	4.50×10^{1}	1.60
320	6.02	3.01×10^{1}	1.44

https://doi.org/10.5194/egusphere-2026-1928
Preprint. Discussion started: 29 April 2026

Table 3. Effective rate constants (k_{eff}, in sec^{-1}) for anti-CH_3CHOO + HONO + WM reaction within the temperature range of 213–320 K, with WM at 20% and 100% relative humidity (RH).

Temp.	$k_{eff}^{RH=20\%}$	$k_{eff}^{RH=100\%}$	k_{eff}^{uncat}
213	1.75×10^{2}	8.74×10^{2}	8.38
216	1.51×10^{2}	7.57×10^{2}	8.39
219	1.31×10^{2}	6.55×10^{2}	8.39
224	1.05×10^{2}	5.23×10^{2}	8.39
235	6.73×10^{1}	3.36×10^{2}	8.32
250	3.69×10^{1}	1.85×10^{2}	8.13
259	2.64×10^{1}	1.32×10^{2}	7.97
265	2.13×10^{1}	1.07×10^{2}	7.85
278	1.36×10^{1}	6.82×10^{1}	7.55
280	1.20×10^{1}	5.98×10^{1}	7.50
290	7.95	3.97×10^{1}	7.23
298	5.79	2.89×10^{1}	7.01
300	5.35	2.68×10^{1}	6.95
310	3.68	1.84×10^{1}	6.65
320	2.55	1.27×10^{1}	6.35

https://doi.org/10.5194/egusphere-2026-1928
Preprint. Discussion started: 29 April 2026

Table 4. Effective rate constants (k_{eff}, in sec^{-1}) for syn-CH_3CHOO + HONO + WM reaction within the temperature range of 213–320 K, with WM at 20% and 100% relative humidity (RH).

Temp.	$k_{eff}^{RH=20\%}$	$k_{eff}^{RH=100\%}$	k_{eff}^{uncat}
213	4.86×10^{2}	2.43×10^{3}	8.17×10^{-1}
216	4.31×10^{2}	2.15×10^{3}	8.12×10^{-1}
219	3.59×10^{2}	1.80×10^{3}	8.08×10^{-1}
224	2.99×10^{2}	1.49×10^{3}	7.98×10^{-1}
235	1.75×10^{2}	8.77×10^{2}	7.73×10^{-1}
250	9.27×10^{1}	4.64×10^{2}	7.29×10^{-1}
259	6.56×10^{1}	3.28×10^{2}	7.01×10^{-1}
265	5.24×10^{1}	2.62×10^{2}	6.80×10^{-1}
278	3.26×10^{1}	1.63×10^{2}	6.36×10^{-1}
280	2.83×10^{1}	1.41×10^{2}	6.29×10^{-1}
290	1.83×10^{1}	9.13×10^{1}	5.94×10^{-1}
298	1.32×10^{1}	6.60×10^{1}	5.66×10^{-1}
300	1.22×10^{1}	6.10×10^{1}	5.59×10^{-1}
310	8.29	4.15×10^{1}	5.25×10^{-1}
320	5.63	2.82×10^{1}	4.92×10^{-1}

https://doi.org/10.5194/egusphere-2026-1928
Preprint. Discussion started: 29 April 2026

References

Alam, M. S., Camredon, M., Rickard, A. R., Carr, T., Wyche, K. P., Hornsby, K. E., Monks, P. S., and Bloss, W. J.: Total radical yields from tropospheric ethene ozonolysis, Phys. Chem. Chem. Phys., 13, 11 002–11 015, 2011.

Alicke, B., Geyer, A., Hofzumahaus, A., Holland, F., Konrad, S., Pätz, H., Schäfer, J., Stutz, J., Volz-Thomas, A., and Platt, U.: OH formation by HONO photolysis during the BERLIOZ experiment, J. Geophys. Res., 108, PHO–3, 2003.

Aloisio, S. and Francisco, J.: Existence of a Hydroperoxy and Water ($HO_2^{\bullet}$-H_2O) Radical Complex, J. Phys. Chem. A, 102, 1899–1902, 1998.

Anand, V. J., Rai, P. K., and Kumar, P.: Criegee + HONO reaction: a bimolecular sink of Criegee, and the missing non-photolytic source of $OH^{\bullet}$, Atmos. Chem. Phys., 25, 16 713–16 727, https://doi.org/10.5194/acp-25-16713-2025, 2025.

Anglada, J. M., Hoffman, G. J., Slipchenko, L. V., M. Costa, M., Ruiz-Lopez, M. F., and Francisco, J. S.: Atmospheric significance of water clusters and ozone–water complexes, J. Phys. Chem. A, 117, 10 381–10 396, 2013.

Aumont, B., Chervier, F., and Laval, S.: Contribution of HONO sources to the NOx/HOx/O_3 chemistry in the polluted boundary layer, Atmos. Environ., 37, 487–498, 2003.

Barker, J., Nguyen, T., Stanton, J., Aieta, C., Ceotto, M., Gabas, F., Kumar, T., Li, C., Lohr, L., Maranzana, A., et al.: MultiWell-2021 Software Suite; J. R. Barker, University of Michigan, Ann Arbor, Michigan, USA, http://claspresearch.engin.umich.edu/multiwell/ (accessed march 5, 2025), 2021.

Bey, I., Jacob, D. J., Yantosca, R. M., Logan, J. A., Field, B. D., Fiore, A. M., Li, Q., Liu, H. Y., Mickley, L. J., and Schultz, M. G.: Global modeling of tropospheric chemistry with assimilated meteorology: Model description and evaluation, J. Geophys. Res.: Atmos., 106, 23 073–23 095, https://doi.org/https://doi.org/10.1029/2001JD000807, 2001.

Buszek, R. J., Francisco, J. S., and Anglada, J. M.: Water effects on atmospheric reactions, Int. Rev. Phys. Chem., 30, 335–369, 2011.

Buszek, R. J., Barker, J. R., and Francisco, J. S.: Water effect on the OH + HCl reaction, J. Phys. Chem. A, 116, 4712–4719, 2012.

Christensen, L. E., Okumura, M., Sander, S. P., Friedl, R. R., Miller, C. E., and Sloan, J. J.: Measurements of the Rate Constant of HO_2 + NO_2 + N_2 $\longrightarrow$ HO_2NO_2 + N_2 Using Near-Infrared Wavelength-Modulation Spectroscopy and UV- Visible Absorption Spectroscopy, J. Phys. Chem. A, 108, 80–91, 2004.

Donahue, N. M., Drozd, G. T., Epstein, S. A., Presto, A. A., and Kroll, J. H.: Adventures in ozoneland: down the rabbit-hole, Phys. Chem. Chem. Phys., 13, 10 848–10 857, 2011.

Emmerson, K. and Carslaw, N.: Night-time radical chemistry during the TORCH campaign, Atmos. Environ., 43, 3220–3226, 2009.

Frisch, M. J., Trucks, G. W., Schlegel, H. B., Scuseria, G. E., Robb, M. A., Cheeseman, J. R., Scalmani, G., Barone, V., Petersson, G. A., Nakatsuji, H., Li, X., Caricato, M., Marenich, A. V., Bloino, J., Janesko, B. G., Gomperts, R., Mennucci, B., Hratchian, H. P., Ortiz, J. V., Izmaylov, A. F., Sonnenberg, J. L., Williams-Young, D., Ding, F., Lipparini, F., Egidi, F., Goings, J., Peng, B., Petrone, A., Henderson, T., Ranasinghe, D., Zakrzewski, V. G., Gao, J., Rega, N., Zheng, G., Liang, W., Hada, M., Ehara, M., Toyota, K., Fukuda, R., Hasegawa, J., Ishida, M., Nakajima, T., Honda, Y., Kitao, O., Nakai, H., Vreven, T., Throssell, K., Montgomery, Jr., J. A., Peralta, J. E., Ogliaro, F., Bearpark, M. J., Heyd, J. J., Brothers, E. N., Kudin, K. N., Staroverov, V. N., Keith, T. A., Kobayashi, R., Normand, J., Raghavachari, K., Rendell, A. P., Burant, J. C., Iyengar, S. S., Tomasi, J., Cossi, M., Millam, J. M., Klene, M., Adamo, C., Cammi, R., Ochterski, J. W., Martin, R. L., Morokuma, K., Farkas, O., Foresman, J. B., and Fox, D. J.: Gaussian~16 Revision C.01, gaussian Inc. Wallingford CT, 2016.

https://doi.org/10.5194/egusphere-2026-1928
Preprint. Discussion started: 29 April 2026

Gao, Q., Shen, C., Zhang, H., Long, B., and Truhlar, D. G.: Quantitative kinetics reveal that reactions of HO_2 are a significant sink for aldehydes in the atmosphere and may initiate the formation of highly oxygenated molecules via autoxidation, Phys. Chem. Chem. Phys., 26, 16 160–16 174, https://doi.org/10.1039/D4CP00693C, 2024.

Geyer, A., Bächmann, K., Hofzumahaus, A., Holland, F., Konrad, S., Klüpfel, T., Pätz, H.-W., Perner, D., Mihelcic, D., Schäfer, H.-J., et al.: Nighttime formation of peroxy and hydroxyl radicals during the BERLIOZ campaign: Observations and modeling studies, J. Geophys. Res. Atmos., 108, 2003.

Gligorovski, S., Strekowski, R., Barbati, S., and Vione, D.: Environmental Implications of Hydroxyl Radicals ($OH^{\bullet}$), Chem. Rev., 115, 13 051–13 092, https://doi.org/10.1021/cr500310b, 2015.

Griffith, S. M., Hansen, R., Dusanter, S., Michoud, V., Gilman, J., Kuster, W., Veres, P., Graus, M., De Gouw, J., Roberts, J., et al.: Measurements of hydroxyl and hydroperoxy radicals during CalNex-LA: Model comparisons and radical budgets, J. Geophys. Res. Atmos., 121, 4211–4232, 2016.

Heard, D. E. and Pilling, M. J.: Measurement of OH and HO_2 in the Troposphere, Chem. Rev., 103, 5163–5198, https://doi.org/10.1021/cr020522s, 2003.

Hermans, I., Nguyen, T. L., Jacobs, P. A., and Peeters, J.: Tropopause Chemistry Revisited: $HO_2^{\bullet}$-Initiated Oxidation as an Efficient Acetone Sink, J. Am. Chem. Soc., 126, 9908–9909, https://doi.org/10.1021/ja0467317, 2004.

Kroll, J. H., Hanisco, T. F., Donahue, N. M., Demerjian, K. L., and Anderson, J. G.: Accurate, direct measurements of OH yields from gas-phase ozone-alkene reactions using an in situ LIF Instrument, Geophys. Res. Lett., 28, 3863–3866, https://doi.org/https://doi.org/10.1029/2001GL013406, 2001.

Kumar, A. and Kumar, P.: Gas phase acidity of water clusters, Phys. Chem. Chem. Phys., 24, 18 236–18 244, https://doi.org/10.1039/D2CP01578A, 2022.

Kumar, A., Mallick, S., and Kumar, P.: Effect of water on the oxidation of CO by a Criegee intermediate, Phys. Chem. Chem. Phys., 22, 21 257–21 266, 2020.

Kumar, A., Mallick, S., and Kumar, P.: Nitrous acid (HONO) as a sink of the simplest Criegee intermediate in the atmosphere, Phys. Chem. Chem. Phys., 24, 7458–7465, https://doi.org/10.1039/D1CP03605J, 2022.

Kumar, M., Sinha, A., and Francisco, J. S.: Role of double hydrogen atom transfer reactions in atmospheric chemistry, Acc. Chem. Res., 49, 877–883, 2016.

Kumar, P. and Sathyamurthy, N.: An ab initio quantum chemical investigation of the structure and stability of ozone-water complexes, Chem. Phys., 415, 214–221, 2013.

Lelieveld, J., Dentener, F., Peters, W., and Krol, M.: On the role of hydroxyl radicals in the self-cleansing capacity of the troposphere, Atmos. Chem. Phys., 4, 2337–2344, 2004.

Lelieveld, J., Gromov, S., Pozzer, A., and Taraborrelli, D.: Global tropospheric hydroxyl distribution, budget and reactivity, Atmos. Chem. Phys., 16, 12 477–12 493, 2016.

Lester, M. I. and Klippenstein, S. J.: Unimolecular decay of Criegee intermediates to OH radical products: Prompt and thermal decay processes, Acc. Chem. Res., 51, 978–985, 2018.

Lin, L.-C., Chang, H.-T., Chang, C.-H., Chao, W., Smith, M. C., Chang, C.-H., Lin, J. J.-M., and Takahashi, K.: Competition between H_2O and $(H_2O)_2$ reactions with CH_2OO/CH_3CHOO, Phys. Chem. Chem. Phys., 18, 4557–4568, 2016.

Luo, P.-L., Chung, C.-A., and Lee, Y.-P.: Rate coefficient of the reaction $CH_2OO + NO_2$ probed with a quantum-cascade laser near 11 μm, Phys. Chem. Chem. Phys., 21, 17 578–17 583, 2019.

https://doi.org/10.5194/egusphere-2026-1928
Preprint. Discussion started: 29 April 2026

Mauldin Iii, R., Berndt, T., Sipilä, M., Paasonen, P., Petäjä, T., Kim, S., Kurtén, T., Stratmann, F., Kerminen, V.-M., and Kulmala, M.: A new atmospherically relevant oxidant of sulphur dioxide, Nature, 488, 193–196, 2012.

Nakajima, M. and Endo, Y.: Communication: Spectroscopic characterization of an alkyl substituted Criegee intermediate syn-CH_3CHOO through pure rotational transitions, J. Chem. Phys., 140, 011 101, 2014.

Nakajima, M., Yue, Q., and Endo, Y.: Fourier-transform microwave spectroscopy of an alkyl substituted Criegee intermediate anti-CH_3CHOO, J. Mol. Spectrosc., 310, 109–112, https://doi.org/https://doi.org/10.1016/j.jms.2014.11.004, spectroscopy of Radicals and Ions in Memory of Marilyn Jacox, 2015.

Newland, M. J., Nelson, B. S., Muñoz, A., Ródenas, M., Vera, T., Tárrega, J., and Rickard, A. R.: Trends in stabilisation of Criegee intermediates from alkene ozonolysis, Phys. Chem. Chem. Phys., 22, 13 698–13 706, https://doi.org/10.1039/D0CP00897D, 2020.

Nguyen, T. L., Lee, H., Matthews, D. A., McCarthy, M. C., and Stanton, J. F.: Stabilization of the Simplest Criegee Intermediate from the Reaction between Ozone and Ethylene: A High-Level Quantum Chemical and Kinetic Analysis of Ozonolysis, J. Phys. Chem. A, 119, 5524–5533, https://doi.org/10.1021/acs.jpca.5b02088, 2015.

Novelli, A., Vereecken, L., Lelieveld, J., and Harder, H.: Direct observation of OH formation from stabilised Criegee intermediates, Phys. Chem. Chem. Phys., 16, 19 941–19 951, 2014.

Onel, L., Lade, R., Mortiboy, J., Blitz, M. A., Seakins, P. W., Heard, D. E., and Stone, D.: Kinetics of the gas phase reaction of the Criegee intermediate CH_2OO with SO_2 as a function of temperature, Phys. Chem. Chem. Phys., 23, 19 415–19 423, 2021.

Pansini, F., Neto, A., and Varandas, A.: Extrapolation of Hartree–Fock and multiconfiguration self-consistent-field energies to the complete basis set limit, Theor. Chem. Acc., 135, 1–6, 2016.

Pawar, P. V., Mahajan, A. S., and Ghude, S. D.: HONO chemistry and its impact on the atmospheric oxidizing capacity over the Indo-Gangetic Plain, Sci. Total Environ., p. 174604, 2024.

Rai, P. K. and Kumar, P.: HO2 radical, a crucial sink of furfural in the atmosphere, Phys. Chem. Chem. Phys., 27, 16 831–16 841, https://doi.org/10.1039/D5CP01593F, 2025a.

Rai, P. K. and Kumar, P.: Influence of Water on the NO_3 + HO_2 Reaction, J. Phys. Chem. A, 129, 2067–2076, 2025b.

Ren, X., Harder, H., Martinez, M., Lesher, R. L., Oliger, A., Shirley, T., Adams, J., Simpas, J. B., and Brune, W. H.: HOx concentrations and OH reactivity observations in New York City during PMTACS-NY2001, Atmos. Environ., 37, 3627–3637, 2003.

Varandas, A. and Pansini, F.: Narrowing the error in electron correlation calculations by basis set re-hierarchization and use of the unified singlet and triplet electron-pair extrapolation scheme: Application to a test set of 106 systems, J. Chem. Phys., 141, 224 113, 2014.

Varandas, A. J.: Odd-hydrogen: An account on electronic structure, kinetics, and role of water in mediating reactions with atmospheric ozone. Just a catalyst or far beyond?, Int. J. Quant. Chem., 114, 1327–1349, 2014.

Vereecken, L.: The reaction of Criegee intermediates with acids and enols, Phys. Chem. Chem. Phys., 19, 28 630–28 640, https://doi.org/10.1039/C7CP05132H, 2017.

Vereecken, L., Harder, H., and Novelli, A.: The reaction of Criegee intermediates with NO, RO_2, and SO_2, and their fate in the atmosphere, Phys. Chem. Chem. Phys., 14, 14 682–14 695, 2012.

Vereecken, L., Harder, H., and Novelli, A.: The reactions of Criegee intermediates with alkenes, ozone, and carbonyl oxides, Phys. Chem. Chem. Phys., 16, 4039–4049, https://doi.org/10.1039/C3CP54514H, 2014.

Vereecken, L., Novelli, A., and Taraborrelli, D.: Unimolecular decay strongly limits the atmospheric impact of Criegee intermediates, Phys. Chem. Chem. Phys., 19, 31 599–31 612, 2017.

Viegas, L. P. and Varandas, A. J.: Can water be a catalyst on the HO_2 + H_2O + O_3 reactive cluster?, Chem. Phys., 399, 17–22, 2012.

https://doi.org/10.5194/egusphere-2026-1928
Preprint. Discussion started: 29 April 2026

449 Weinstock, B.: Carbon monoxide: Residence time in the atmosphere, Science, 166, 224–225, 1969.